Ultrasonics 135 (2023) 107115

Contents lists available at ScienceDirect

Ultrasonics

journal homepage: www.elsevier.com/locate/ultras

Rapid quantification of 3D ultrasound fields with wavefront sensing and Schlieren tomography

Mateu Colom [a], Pietro Ricci [a], Martí Duocastella [a,b,*]

[a] Department of Applied Physics, Universitat de Barcelona, C/Martí i Franquès 1, 08028 Barcelona, Spain
[b] Institut de Nanociència i Nanotecnologia (IN2UB), Av. Diagonal 645, 08028 Barcelona, Spain

ARTICLE INFO

Keywords:
Schlieren technique
Ultrasound characterization
Wavefront sensing
Tomography
Three-dimensional pressure field

ABSTRACT

The rapid and precise characterization of three-dimensional (3D) pressure fields inside water is paramount for ultrasound (US) applications in fields as relevant as biomedicine and acoustic trapping. The most conventional way is to scan point-by-point a needle hydrophone across the field of interest, which is an intrinsically invasive and slow process. With typical acquisition times of hours and even days, this method remains impractical in many realistic scenarios. Alternatively, optical techniques can be used to non-invasively and rapidly measure the changes in light intensity or phase induced by pressure differences. However, these techniques remain largely qualitative: extracting precise pressure values can require extensive calibration, and complex processing, or can be limited to low-pressure ranges. Here, we report how combining wavefront sensing and Schlieren tomography enables rapid and direct quantification of 3D pressure fields while obviating any calibration steps. By simultaneously capturing optical phase and intensity information of the US-perturbed fluid using a Wavefront Sensor and Schlieren projections, respectively, 3D pressure fields over several millimeters cubic can be reconstructed after a few seconds. We present a detailed description of the approach and prove its feasibility by characterizing the US field after an acoustic lens, which is in excellent agreement with calibrated hydrophone measurements and simulations. These results are a significant step forward toward the precise and real-time characterization of ultrasound patterns.

1. Introduction

Recent developments in ultrasound (US)-based methods, ranging from acoustic holography to medical ultrasound, demand techniques capable of rapid and precise measurement of three-dimensional (3D) pressure fields inside liquids [1–7]. Typically, this is achieved by using a needle hydrophone [8] that is scanned, point by point, throughout the pressure field. Such a device, analogous to a microphone but for water immersion, uses a thin piezoelectric film at the needle tip to convert pressure into voltage, allowing simultaneous US amplitude and phase detection. However, its practical implementation faces several drawbacks. First, the presence of the hydrophone can affect the measurements, thus making it an intrinsically invasive technique [9]. Secondly, hydrophones typically exhibit a high directivity, producing measurements with an angular dependence. Thirdly, the resolution is determined by the size of the hydrophone's tip, which can be a limiting factor when small field features need to be characterized. Note that reducing the tip's size can also result in a loss of sensitivity. Finally, one of the biggest downsides is the measurement time, with an average rate of acquisition on the order of 1 voxel per second. Thus, scanning a region of several mm can take some hours or days long [10], rendering this technique ill-suited for applications involving dynamic US fields.

Several approaches have been developed to address these issues. One such example is thermography [11], based on acquiring thermal images of a US-absorbing membrane whose temperature depends on the ultrasound field. While allowing for fast 2D reconstruction of pressure maps, this technique remains invasive, and it only works with continuous US fields, that is, the instantaneous pressure values cannot be measured. Arguably, though, the most promising alternatives to hydrophone measurements are optical methods. As their name indicates, they use changes in the intensity or phase of light to retrieve information about an ultrasound field. They are usually non-invasive and can be broadly classified into two main groups depending on whether they offer quantitative or only qualitative pressure information.

Quantitative optical techniques are normally based on interferometric systems that allow converting the phase information of light into

* Corresponding author.
E-mail address: marti.duocastella@ub.edu (M. Duocastella).

https://doi.org/10.1016/j.ultras.2023.107115
Received 27 April 2023; Received in revised form 21 July 2023; Accepted 24 July 2023
Available online 26 July 2023
0041-624X/© 2023 The Author(s). Published by Elsevier B.V. This is an open access article under the CC BY license (http://creativecommons.org/licenses/by/4.0/).

pressure. For instance, by using a couple of mirrors forming a Fabry-Pérot cavity [12], changes in the optical power reflected through the cavity can be directly correlated with changes in the cavity length caused by pressure waves. In this case, the acquisition time can be faster than hydrophone measurements, but scanning is still needed to retrieve 3D pressure fields, making it an overall long process. Similarly, Michaelson interferometry can be used to locally interrogate pressure fields [13,14], but to retrieve full 3D information of an acoustic field a time-consuming scanning step is still needed. Anyhow, interferometric-based strategies come with the caveat of added complexity in the optical system. Indeed, the alignment of the reference or main beam is critical for accurate measurements, which makes them difficult to implement in practice.

Instead, qualitative optical techniques offer ease of implementation at the cost of restricting the information provided to a qualitative assessment of the pressure field, not exact values. An example includes Scanning Laser Doppler Vibrometry (LDV), which exploits the acousto-optic effect [15,16] to visualize the small variations of the refractive index produced by US [17,18]. Another well-known method based on the acousto-optic effect is the Schlieren technique [19–21]. In this case, the region where the pressure field is to be measured is illuminated with a collimated light beam. Given the non-uniform refractive index induced by US, the beam gets deviated. By placing a knife-edge at the back focal plane of an imaging lens before a camera, such light deviations can be converted into a high-contrast image - the contrast is proportional to the first derivative of the refractive index. Note that, in a single snapshot, a 2D projection of the US field can be obtained. In addition, by combining this technique with a multi-angular visualization system, or simply with a rotating US field, the 3D pressure pattern can be reconstructed via tomography [22].

Efforts have been made to provide quantitative pressure information in Schlieren systems while preserving their core advantages in terms of speed and simplicity. A simple solution is to assume a linear relationship between the intensity of Schlieren contrast fringes and US pressure, but this hypothesis is only valid for weak US fields and the approach requires an initial calibration, that is, an initial pressure measurement using, for example, a needle hydrophone, that serves as a reference [23]. A less restrictive strategy is Background Oriented Schlieren (BOS), where a well-known background is used to quantify the light deflection angle in 2D, and hence, the projected density gradient vector field. However, traditional BOS cannot produce real-time Schlieren images as it requires a post-processing step, the measurements are influenced by the randomness of the background pattern, and it experiences difficulties when detecting displacements of large density gradients due to shape distortion of the random dots. Similarly, the Calibration Color Schlieren (CCS) [24], utilizes a colored background to quantify light deflection, but it suffers from relatively high noise measurements and offers a small dynamic range. Another alternative that uses a Schlieren-like system combines optical phase contrast with acoustic holography simulations [25], but they still may need an initial calibration and are not suitable for high-pressure fields, where phase unwrapping is needed. Simply put, an easy-to-implement optical method that allows the rapid quantification of 3D ultrasound fields in water without any calibration steps does not exist.

In this work, we fill this void and present an interferometric-free optical method based on a Toepler-Schlieren setup parallel to a wavefront detection system. The wavefront sensor (WFS) is used to directly quantify the phase projection field of the US pattern within a small field of view. These values are inferred from the Schlieren images as both sensors (Schlieren camera and WFS) are centered on the same region, but the Schlieren setup field of view is larger than that of the WFS. Because phase differences are just refractive index differences multiplied by the distance of light-US interaction, the refractive index values are straightforwardly obtained. By rotating the. Finally, using the piezo-optic coefficient of water and capturing the projections at different angles by rotating the US emitting source, the 3D pressure map is reconstructed. It is important to stress that this method does not need any kind of hydrophone calibration, does not require any symmetry of the pressure field, and is suitable for US characterization in any media as long as it is optically transparent. This technique has been tested with a focused US field created by a PDMS convex lens placed on top of a flat piezoelectric disk. The obtained 3D reconstructed pattern is in excellent agreement with the measured hydrophone values and with the corresponding numerical simulations.

2. Fundamentals of Schlieren tomography and WFS

The gist of our calibration-free US measurement system is the combination of a Schlieren tomography setup with a quantitative optical phase retrieval method. For the latter, we selected a Shack-Hartman WFS, based on an array of microlenses placed in front of a camera sensor. Widely used in adaptive optics and ophthalmology [26,27], a WFS enables direct capture of the phase information of a light beam without the need for interferometric schemes. Such configuration also allows measurements of large phase differences – typically, above 20π – rendering it suitable for working with large pressure values. Note that optical phase values can be converted into refractive index changes, and, in turn, pressure values provided the optical path length, and the piezo-optic coefficient of water are known. The main problem of a WFS is the tradeoff between spatial resolution and field of view. Because the number of microlenses is typically low, in the order of 100 × 100, the consequent low number of measured points impedes the quantification of US fields over a large field of view. To address this issue, we use the projections from a Schlieren tomography setup that allows measuring many points, only limited by the particular camera sensor used – in the order of 1000 × 1000 pixels. Thus, by simultaneously capturing information with the WFS and the Schlieren system, we can directly relate optical phase values obtained with the former with the light intensity measured with the latter. Such information is sufficient to reconstruct the entire 3D pressure field using computational tomography based on a step-by-step rotation of the US field. Importantly, because the role of the WFS is to provide an instantaneous readout of the phase information, no calibration is needed, and the speed at which the US field can be characterized only depends on the camera frame rate and US-rotation speed. In addition, the use of synchronized pulsed illumination with the US allows capturing a frozen-in-time ultrasound pattern. Therefore, by changing the delay time between US and light pulses, it is possible to characterize the 3D pressure field at any given time.

A mathematical expression of the role of each of the main components of our system can provide further insights into its working principle. Regarding the WFS, each of the microlenses provides a measurement of the average wavefront slope (over the lensed area) based on the location of the focal spot on the sensor. When the collimated light beam is distorted by the US and reaches the WFS, the beam wavefront $w(x,z)$ slopes can be written as:

$$S_x = \frac{\partial w(x,z)}{\partial x},\ S_z = \frac{\partial w(x,z)}{\partial z} \tag{1}$$

where x and z correspond to horizontal and vertical directions relative to the camera plane. By integrating the wavefront slopes in both directions, the value of $w(x,z)$ can be obtained, which corresponds to the projected phase values $\Delta\varphi$. Instead, the Schlieren setup measures changes in light intensity caused by changes in the refractive index n of a medium given by [28]:

$$\frac{\Delta I}{I} \cong \frac{f_{FL2}}{a}\int_{s_1}^{s_2}\frac{1}{n_o}\frac{\partial n}{\partial z}dy \tag{2}$$

where f_{FL2} is the focal length of the image-forming lens, a is the size of the spot at the position of the knife edge, s_1 and s_2 limit the region where the medium is perturbed, z is the direction perpendicular to the knife edge, n_o is the refractive index of the unperturbed medium, and y is the

light propagation direction. From Eq. (2) it can be seen that this Schlieren method is sensitive to the first derivative of the refractive index in the direction perpendicular to the knife edge. Thus, the camera collects an image of a projection of the refractive index derivatives along the propagation axis. Note that it is typically not possible to solve this equation given that the integral limits are unknown, which renders Schlieren a mainly qualitative measuring technique. Importantly, by integrating the Schlieren image along the knife-edge direction, a projected image whose contrast is proportional to the refractive index is obtained. We can express this mathematically as:

$$\int \frac{\Delta I(x,z)}{I} dz \cong \frac{f_{FL2}}{a\, n_o} \int \frac{\partial n(x,z)_{proj.}}{\partial z} dz \propto n(x,z)_{proj.} \tag{3}$$

where z is the direction perpendicular to the knife edge orientation. Such an image is also proportional to the projected phase values of light passing through the US-modulated medium, also measured with the WFS ($n(x,z)_{proj.} \propto w(x,\ z)$). Therefore, by comparing the integrated Schlieren image with the WFS-measured phase map, we can directly assign phase values to intensity differences:

$$\int \frac{\Delta I(x,z)}{I} dz = C\, w(x,z) = C\, \Delta\phi\left(x,z\right) \tag{4}$$

where C is a proportionality constant. Such a comparison acts as an in-situ calibration step. In other words, determining the value of C allows the integral of the captured Schlieren image to be converted into a quantitative phase map.

With this information, it is then possible to retrieve the 3D pressure field by applying computational tomography. Specifically, we first reconstruct the 3D phase map by rotating the US source, sequentially acquiring a series of Schlieren images, and solving the inverse computational problem of tomography. The 3D phase map contains information on the phase difference caused by the pressure field, which can be written as:

$$\Delta\phi = \frac{2\pi}{\lambda} \Delta n\, L \tag{7}$$

where λ is the wavelength of light, L is the voxel length of the reconstructed map and Δn the refractive index change at each voxel. Once Δn is known, the individual voxel pressure values P (relative to atmospheric pressure) can be calculated using the piezo-optic coefficient for water, C_{PO}, at 20 °C [29] as:

$$\Delta n = C_{PO}\, P \tag{8}$$

where C_{PO} is $1.51{\cdot}10^{-10}$ Pa^{-1}. The pressure-refractive index relation behaves linearly even for extremely high pressures, so this coefficient is considered constant for our experiments.

3. Materials and methods

3.1. Experimental setup

Fig. 1a shows a scheme of the setup presented here. The light emitted by the point light source (LED OD-469L, Opto Diode Corp, $\lambda = 469$ nm) is first homogenized by using a glass diffuser DF (DG10-1500 N-BK7, Thorlabs). This allows removing the internal structure of the LED. The condenser lens CL (plano-convex lens LA1951 (Thorlabs), focal length = 25.4 mm) focuses the light beam to a 1 mm diameter pinhole, and the first field lens, FL_1 (plano-convex lens LA1986 (Thorlabs), focal length = 125 mm), collimates the light beam into the water tank (WT), filled with distilled water.

A flat piezoelectric disk (PIC-181, PI Ceramic GmbH) with a diameter of 25 mm, a thickness of 1 mm, and a resonance frequency of 2.2 MHz is used as the ultrasonic emitter. The initial flat pressure distribution is then focused by a convex acoustic lens, with a diameter of 25 mm and a focal distance of 30 mm, which was manufactured in the lab using PDMS (Sylgard™ 184, Dow Inc.). The piezoelectric disk is driven by a Waveform Generator WG (SDG6022X, SIGLENT) with a sinusoidal signal, whose voltage is amplified using a High-Power Amplifier (ZHL-1–2W+, Mini-Circuits). The sinusoidal excitation was tuned in a burst mode (burst rate of 2.5 kHz, 30 cycles/burst) to measure only the instantaneous emission and avoid the visualization of reflections on the tank walls and wave interference. The US emission is synchronized with the light emission (see Fig. 1b) in such a way that the central part of the 30 emitted cycles fits in the center of the light beam. This is done by adjusting the correct delay between the LED trigger and the US trigger emitted by the Pulse Generator (9520 Series, Quantum Composers), which in our case is around 32 μs. Since the LED light pulse has a duration of 50 ns, which is one order of magnitude smaller than the typical period of the measured US waves, hence frozen-in-time emissions are acquired. After the interaction of the collimated beam with the ultrasound field, the perturbed beam is divided into two light paths by a 50:50 beamsplitter cube, BSC (BS031, Thorlabs).

3.2. Phase-shift measurement

Part of the light beam is deviated by the BSC and then reflected by a mirror (BB1-E02, Thorlabs) into a *4f* system composed by L_1 (bi-convex lens LB1437, focal distance of 150 mm, Thorlabs) and L_2 (plano-convex lens LA1908, focal distance of 500 mm, Thorlabs) that magnifies the beam of factor 10/3. The collimated beam reaches the WFS (Shack-Hartmann Wavefront Sensor, Dynamic Optics Srl.), and encounters an array of microlenses (60 × 48 lenses with a diameter of 140 μm each one and a separation of 150 μm between lenses). After this array, the sensor (MER2-230-168U3M) measures the light focused by the microlenses distributed in a 2D pattern of points. The displacements of these points with respect to the reference positions without perturbation correspond to the wavefront slopes. By integrating these wavefront gradients in both x and z directions, the projected phase distribution is obtained. Due to the beam magnification, the obtained field of view is 2.3 mm × 1.85 mm. When performing a measurement, the undisturbed wavefront does not need to be perfectly flat, as background subtractions are applied to consider the undistorted phase distribution.

The upper limit of detection of our setup is fundamentally given by the point where the relationship between pressure and refractive index becomes non-linear (above 100 MPa). In practice, though, there is a lower detection limit that depends on the wavefront sensor geometrical parameters, namely the diameter of the lenses and their focal lengths (150 μm and 3.74 mm, respectively). Such a limit corresponds to the maximum phase difference that can be resolved with the WFS. Considering the maximum measurable projected phase to be $\pm\ 8{\cdot}10^{-6}$ m (corresponding to a $\pm\ 34\pi$ phase difference), the corresponding maximum measurable projected pressure for our US pattern geometry is ± 1200 MPa, and the reconstructed 3D pressure value maximum is ± 50 MPa.

3.3. Schlieren measurement and reconstruction

The non-reflected light beam coming from the beam splitter reaches the second field lens, FL_2 (bi-convex lens LA1779, focal length = 300 mm, Thorlabs), located at a distance of 1200 mm from the US focusing region. At the back focal plane of FL_2 a horizontal knife edge is positioned to block half of the light spot. The unblocked light reaches the CMOS camera (CS165MU1 - Zelux® 1.6 MP Monochrome, Thorlabs), whose sensor has a resolution of 3.45 μm/pixel. The camera is located at the image plane (400 mm from FL_2), and therefore there is a magnifying factor of 1/3, which defines a field of view of 14.1 mm × 10.5 mm. A 2 × 2 binning is applied to increase the signal-to-noise ratio.

The US generation system rotated with the help of a rotatory stage (PRM1/MZ8, Thorlabs), and consequently, a projected image of the US field is obtained at a certain angular direction. The camera acquisition is synchronized with the rotatory stage, so we know exactly the angular

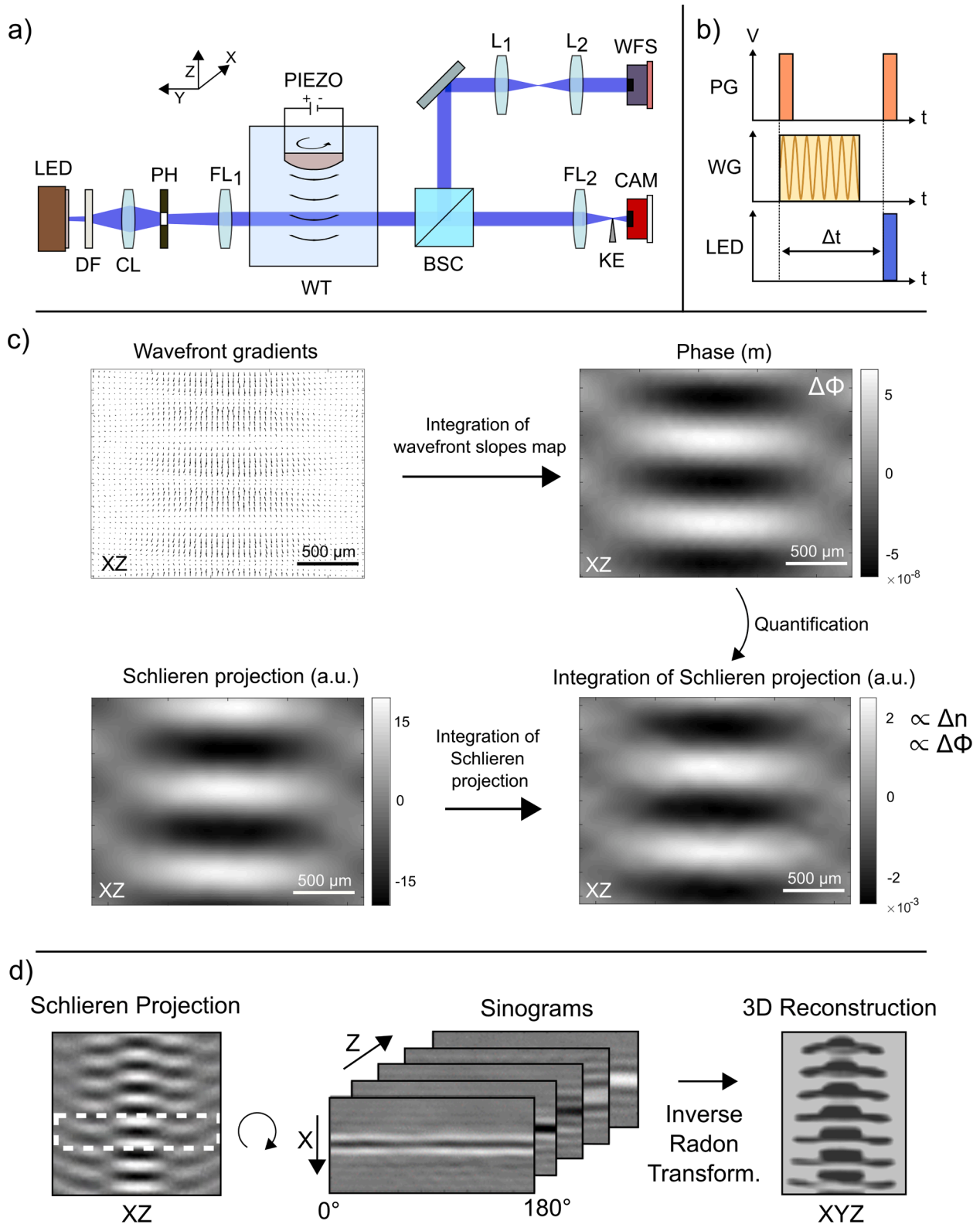


Fig. 1. Principle of the Schlieren-WFS system for rapid calibration-free US-measurement. (a) Schematic diagram of the Schlieren-WFS setup. DF: diffuser, CL: cylindrical lens; PH: pinhole; FL1: first lens Schlieren setup; BSC: beam splitter cube; WT: water tank; FL2: second lens Schlieren setup; KE: knife edge; CAM: camera; L1: first lens WFS setup; L2: second lens WFS setup; WFS: wavefront sensor. (b) Temporal diagram of the synchronization signals between the ultrasound lens (driven with a sinusoidal signal generated with a Waveform Generator WG) and the LED pulsed illumination. A pulse generator (PG) is used to initiate the acquisition process. (c) Flow diagram of the process for quantitative measurement. From the wavefront slopes measured with the WFS, the optical phase differences $\Delta\phi$ of light passing through the US-modulated medium can be extracted (top). Integrating the projection images obtained with the Schlieren camera, a qualitative image proportional to the phase (and refractive index) is obtained (bottom). (d) Flow diagram of the computational tomographic reconstruction used to extract the 3D pressure field by acquiring multiple quantitative Schlieren projections at different angles.

position at which every projection has been acquired. To get clear projections of the US field and avoid refractive index disturbances that aren't originated by the changes of pressure, a reference frame (background) is taken immediately after a measurement frame. Therefore all inhomogeneities derived from particles in water or other elements on the setup are erased. In such a way, by applying a camera frame rate of 36 Hz and rotating the field at 18°/s, all projections can be recorded in 10 s. Using these parameters, a projection is obtained for each degree for a total of 180 projections. Importantly, the number of projections (*Np*) determines the signal-to-noise ratio (SNR), root mean square error (RMSE), and contrast of the reconstructed field. The RMSE decreases with *Np*, and the contrast and SNR increases with Np. The 180 projections used in experiments herein resulted in an RMSE lower than 0.01 MPa.

The phase projections obtained from the combination of the Schlieren projections and the WFS-phase maps (see Fig. 1c) are processed with MATLAB. The reconstruction of the 3D field consists of the following steps:

- The 3D matrix containing all the 2D projections at different angles is rearranged to obtain a sinogram for each pixel in the vertical axis z.
- Each sinogram, which is a 2D image containing the information of the x axis in all the observed angles, is transformed into the frequency domain using the Fourier transform. The Fourier-transformed projections are then multiplied by a filter function in the frequency domain. The purpose of the filter is to suppress artifacts, enhance the image quality and reduce high-frequency noise. After filtering, the projections are transformed back into the spatial domain using the inverse Fourier transform.
- Once the filtered projections are obtained, they are back-projected into a two-dimensional image. Back projection involves assigning the intensity of each projection pixel to all the corresponding points along the line of projection.
- Finally, all reconstructed 2D images are rearranged on the z axis to obtain the reconstructed 3D pattern.

3.4. Hydrophone measurements

A 0.5 mm needle hydrophone (NH0500, Precision Acoustics, Ltd) was used to measure the US field. As the hydrophone measures the pressure value at a certain point in the space, point-by-point scanning was needed. A three-dimensional XYZ stage (MTM 150 CC1, Newport), properly controlled by a motion controller (ESP301, Newport), is implemented in the setup attached to the piezoelectric-PDMS emitter, while the needle hydrophone remains in a fixed position. This needle position corresponds to the central position of the Schlieren-WFS measurements. Scanning the US field along all the directions a 3D map of the pressure field is acquired. A Data Acquisition Card (PCI digitizer board CS23G8 CobraMax, GaGe Applied), served as a digital oscilloscope to visualize and measure the detected pressure. For this measurement, the Waveform Generator is triggered by the card instead of by the Pulse Generator, so for each stage movement, the instantaneous pressure value is recorded at the same time delay as the Schlieren measurement to ensure the same region inspection. The typically used scan steps are between 0.1 and 0.2 mm.

3.5. Simulations

Numerical simulations are made for the sake of comparison. A MATLAB open-source toolbox called k-Wave is used [30]. This toolbox enables simple and efficient simulation of time-domain wave propagation. The software is designed for time-domain acoustic and ultrasound simulations in complex and tissue-realistic media, and it includes, among other features, an advanced time-domain model of acoustic wave propagation that can account for nonlinearity, acoustic heterogeneities, and power law absorption. The governing equations used in the k-Wave simulation functions are derived directly from the equations of fluid mechanics. The nonlinear terms are then re-written in terms of the acoustic Lagrangian density. If only cumulative nonlinear effects are important, the Lagrangian density can then be set to zero. The strength of the nonlinear effects observed is mainly dependent on the parameter of nonlinearity and the pressure magnitude. If this nonlinearity parameter is given, nonlinear governing equations are solved at each time step. If this is not given, linear governing equations are used. In our case, we do not consider non-linearities, because we work at relatively low pressures, and the simulations obtained with and without the nonlinearity parameter differ by less than a 0.01%, while the speed of the computation gets compromised. Moreover, the simulated pressure pattern that we obtained is in excellent agreement with both the Schlieren-WFS and the hydrophone measurement. We simulated the propagation of the US field with the same parameters and conditions as the experimental setup. To compare the values with the experimental results, the pressure is normalized to the hydrophone measurement maximum value.

4. Results and discussion

4.1. Proof-of-principle of the Schlieren-WFS method

To prove the feasibility of our approach for quantitative ultrasound characterization, we first experimentally measured a focused US field inside distilled water. In more detail, we characterized the instantaneous pressure field around the focal region of an acoustic lens with a numerical aperture of 0.58, a 20 mm focal length, and a base diameter of 25 mm. Thus, the illumination beam of the Schlieren-WFS system passed through the US region exhibiting the highest pressure. Fig. 2a shows the retrieved pressure field along two orthogonal slices. In this case, the driving voltage was 76.4 V, and the driving frequency 2.2 MHz. The retrieved pressure field covered a volume of $10 \times 10 \times 10.5$ mm^3, with $256 \times 256 \times 270$ cubic voxels, each with a size of 40 μm (spatial resolution of the system), and it was acquired within 10 s. This represents a striking measurement rate of 1.77 million points per second. The XY cross-sectional profile of the reconstructed US pattern at $z = 0$ mm exhibits an axisymmetric ring pattern, with a high-pressure central lobe of 0.5 MPa surrounded by low-pressure rings of −0.05 MPa and below. There is a slight distortion of the first rings, probably caused by imperfections in the custom-made PDMS focusing lens. In any case, the central lobe features a full width at half maximum (FWHM) of approximately 1.4 mm, in good agreement with the theoretical value of 1.4 mm corresponding to the acoustic Airy disk diameter. Along the US propagation direction, the pressure field features an axisymmetric distribution with strong lateral confinement and periodic high- and low-pressure regions – also covering a range from 0.5 to −0.5 MPa. The wavelength inferred from this pressure map is 0.67 mm, as expected for the acoustic frequency used.

As a benchmark for our Schlieren-WFS system, we repeated the US measurement of the exact $10 \times 10 \times 10.5$ mm^3 region using a needle hydrophone. We selected a device with a sensitivity of 275 mV/MPa at 2.2 MHz and a measurement uncertainty of 17%. Importantly, we ensured that the US frequency and intensity were the same as in the previous experiment. Given the long measurement time needed by the hydrophone, we arbitrarily chose a spatial resolution of $0.25 \times 0.25 \times 0.15$ mm^3, about 6 times worse than with the Schlieren-WFS system. Still, retrieving the entire 3D pressure field took about 5 h. As shown in Fig. 2a, there is an excellent agreement between the results from our method and the ones from the hydrophone measurement. The high-pressure central lobe at $z = 0$ remains identical, with a value of 0.5 MPa and an FWHM of 1.4 mm. Similarly, the surrounding low-pressure ring feature the same deviations as previously observed. Along the XZ direction, the pressure field remains periodic, with a periodicity of 0.67 mm corresponding to the acoustic frequency. The main difference between the two methods is the pixelization of the results of the

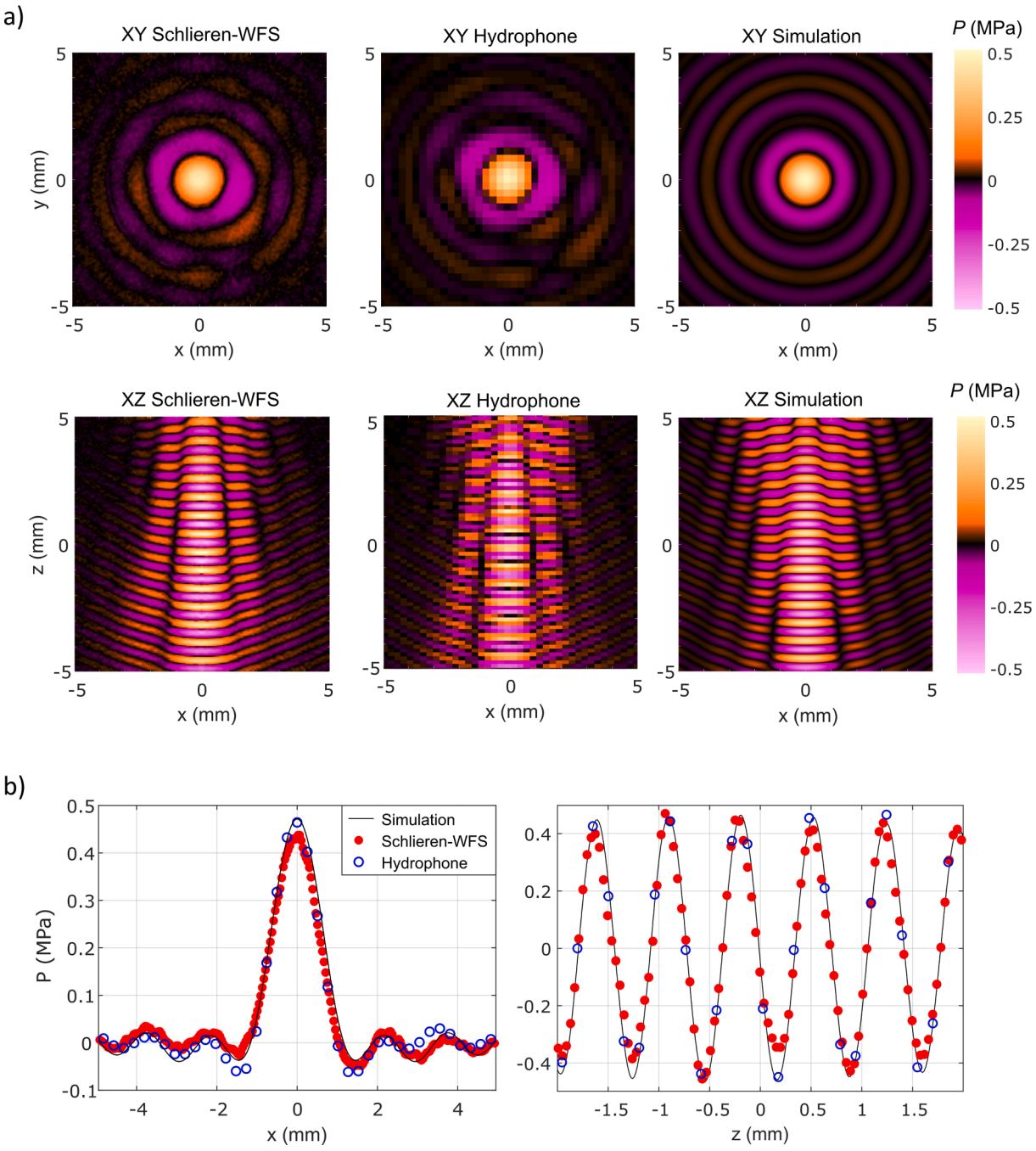


Fig. 2. Experimental measurements and simulations of a 3D US field generated after an acoustic lens. (a) Colormaps of the XY plane and XZ pressure field distributions measured with our Schlieren-WFS system and the classical needle hydrophone, as well as simulations. (b) Plots of the central pressure profiles along the *x*-axis (left) and *z*-axis (right) for the simulated (black), and experimentally measured Schlieren-WFS (red) and hydrophone (blue) pressure fields.

hydrophone, caused by the decrease in spatial resolution. Note, though, that characterizing the US region with the same resolution as with the Schlieren-WFS system would have taken 30 days.

For a more quantitative assessment of our method, we also compared the experimental results with numerical simulations. Specifically, we computed the US field in the vicinity of the focal region of an acoustic lens with the same specifications as the one used in experiments. The simulated values are in very good agreement with both hydrophone and Schlieren-WFS measurements. In fact, the XY cross-sectional profile has the same characteristics as experimental measurements, with a central high-pressure lobe surrounded by low-pressure rings. Interestingly, the symmetry of the simulation is superior to experiment, given the ideal case considered. Also, the US profile along the XZ plane remains periodic, barely distinguishable from experiment. A more refined analysis of these results is shown in Fig. 2b. In this case, we plotted the central profile of the pressure field along the *x* and *z* directions for the simulation and experimental methods considered. Regarding the pressure profile along the *x*-axis, it exhibits, for the three cases analyzed, the characteristic shape of an acoustic Airy disk. Besides the expected lower number of data points corresponding to the hydrophone measurement, they are all very similar, with a root mean square error, relative to simulation, of 5% and 4% for the Schlieren-WFS and hydrophone, respectively. Regarding the *z*-axis profiles, they are also comparable, showing a periodic pressure with a wavelength of 0.67 mm. The root mean square error of the Schlieren-WFS and hydrophone relative to the simulation is 9% and 12%, respectively.

4.2. Pressure measurement at different time instances and US frequencies

The Schlieren-WFS system exhibits a high temporal precision that allows characterizing dynamic pressure fields. The reason lies in the use of short illumination pulses. Thus, despite the relatively long exposure time of the camera employed, the pulsed light enables capturing the acousto-optic interaction at a given time instance. An example of such capability is shown in Fig. 3a. In this case, we characterized the pressure field at the vicinity of the focal region of the acoustic lens described in section 4.1 when driven at 2.2 MHz and at different delay times between the US emission and the LED pulse. At $\Delta t = 22.05$ μs, the US wave has not yet reached the entire observable window of the Schlieren-WFS setup. It requires $\Delta t = 32.05$ μs to achieve so. Notably, an additional delay of only 75 ns leads to observable differences, as shown for $\Delta t = 32.125$ μs, especially across the XY plane. Such a delay corresponds to a displacement of the US wave of only 111 μm, that is, 1/6 of the acoustic wavelength. The fine temporal resolution of our system can be used to reconstruct the propagation of an ultrasonic wave (see Supplementary Fig. S1 Video 1). The entire sequence of images was acquired in less than 2 min.

Similarly, it is possible to characterize pressure fields obtained at different driving frequencies. As shown in Fig. 3b-d, the reconstructed 3D pressure fields at 1 MHz, 2.2 MHz, and 3 MHz exhibit the same trends described above in terms of periodicity along the propagation direction (XZ and YZ slices), and bulls-eye circular pattern in the XY plane. Each of them, though, features distinct pressure values, with the widest range obtained at 2.2 MHz – 1 MPa in total – which corresponds to the resonant frequency of the piezoelectric plate (see section 4.3 for further details). The measurements performed off-resonance exhibit a lower signal-to-noise ratio, and thus the reconstructed fields appear noisier and with lower contrast. Still, it is clearly possible to observe how the acoustic wavelength and the central lobe decrease with driving frequency. In fact, the measured wavelength values of 1.48 mm and 0.49 mm for the 1 MHz and 3 MHz, respectively, are in good agreement with the expected theoretical values. The same occurs with the FWHM of the central lobes – 1.74 mm and 0.96 mm for 1 MHz and 3 MHz, respectively. Videos of the three-dimensional field at 1 MHz, 2.2 MHz (with $\Delta t = 22.05$ μs and $\Delta t = 32.05$ μs) and 3 MHz can be found in the Appendix as Supplementary Videos 2–5, respectively.

4.3. Pressure sensitivity and temporal performance of the Schlieren-WFS system

A central aspect of any US measurement system is the sensitivity to pressure changes, which ultimately determine its usable range. To this end, we first measured the pressure field using the Schlieren-WFS system when driving the piezoelectric disk at 2.2 MHz and different voltage amplitudes. As shown in Fig. 4a, the system exhibits an increasing linear response with voltage. This result is in agreement with the expected trend of a piezoelectric disk, where higher driving voltages lead to higher pressures, as verified with the conventional needle hydrophone. Note the significant difference in terms of measurement errors for the two systems. The Schlieren-WFS system exhibits a similar uncertainty for all driving voltages of about ± 0.05 MPa, as calculated using the

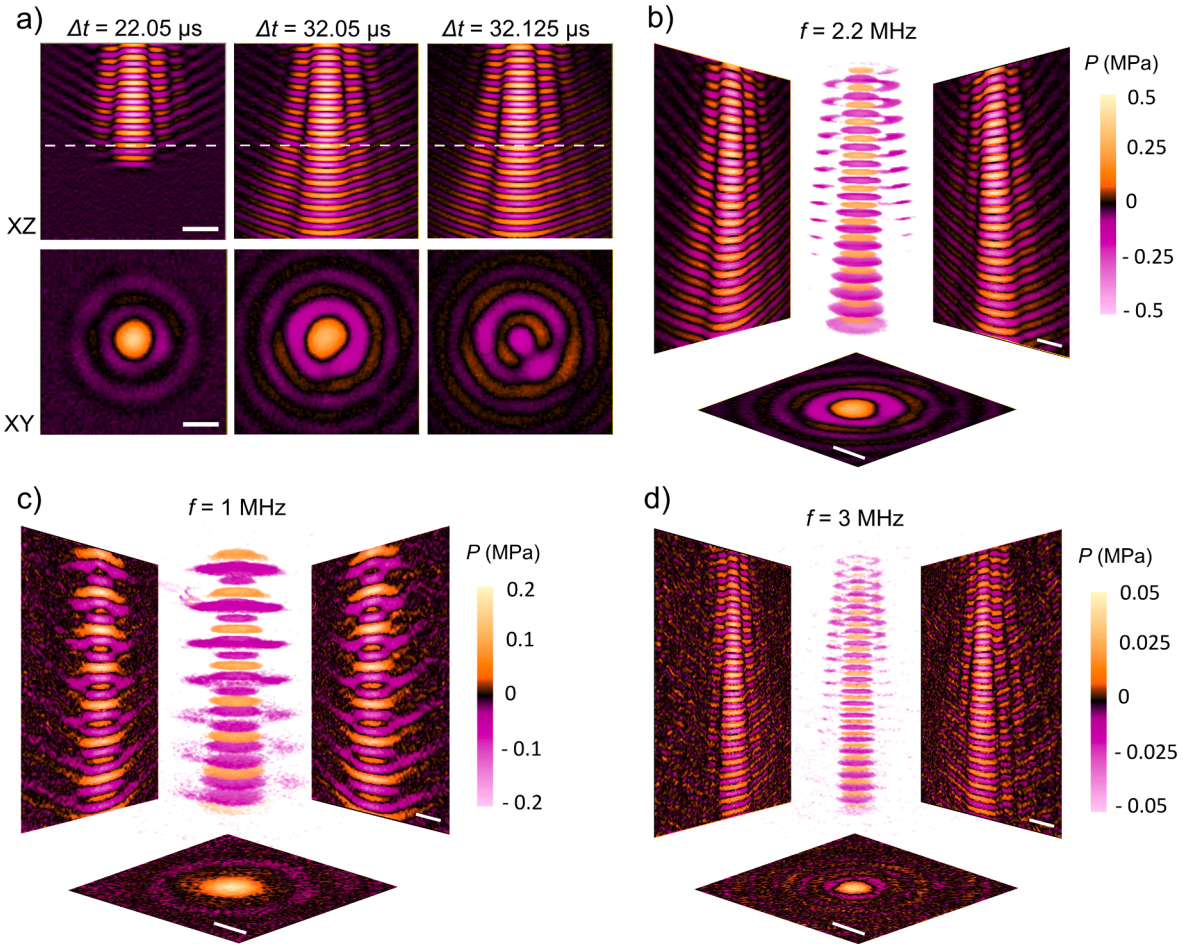


Fig. 3. Measurements of different US fields using the Schlieren-WFS setup. (a) XZ (top) and XY (bottom) pressure maps of the reconstructed pressure field for delay time $\Delta t = 22.05$ μs (left), $\Delta t = 32.05$ μs (center), and $\Delta t = 32.125$ μs (right). The white dashed lines indicate the z position taken for the XY images. The scale bar represents 2 mm. (b-d) 3D reconstructions of the US field for a frequency of 2.2 MHz, 1 MHz, and 3 MHz, respectively. The scale bar represents 2 mm.

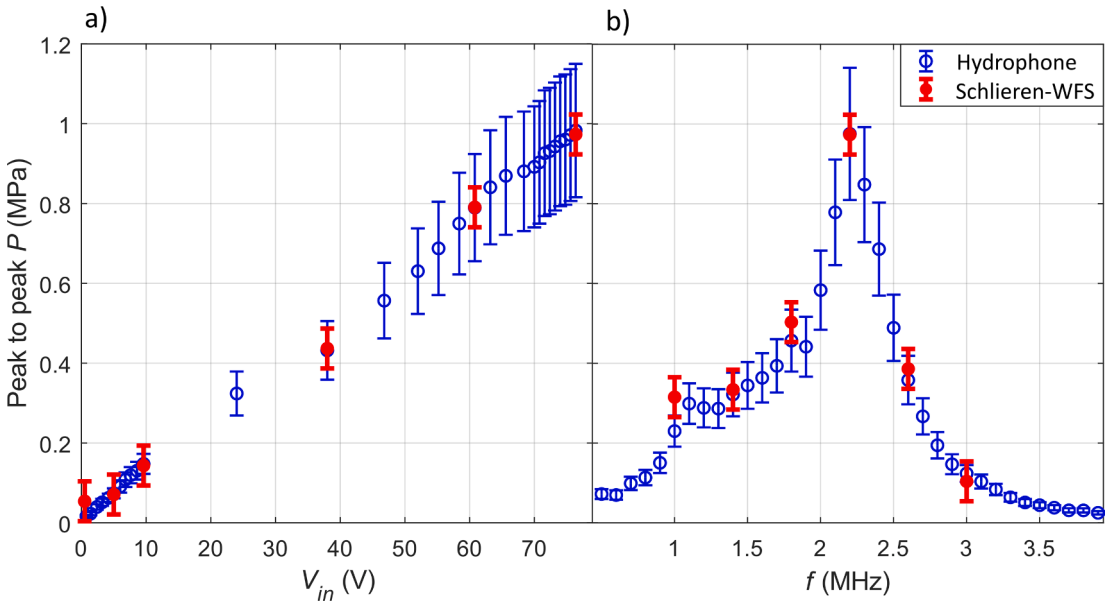


Fig. 4. Pressure sensitivity of the Schlieren-WFS system. (a) Plot of peak-to-peak pressure at 2.2 MHz measured with the needle hydrophone (blue circles) and Schlieren-WFS system (red circles) as a function of the driving voltage of the piezoelectric disk used to generate the US waves. (b) Plot of the experimental peak-to-peak pressure measured with the needle hydrophone (blue circles) and Schlieren-WFS system (red circles) at different pressure values and driving voltage of 76 V.

standard deviation of 5 different measurements for each case. Instead, the needle hydrophone presents a 17% uncertainty in a frequency range between 1 and 12 MHz, as specified by the manufacturer. Therefore, while both systems are sensitive over a large pressure range, the Schlieren-WFS offers higher precision at larger pressures.

Analogous conclusions can be extracted by measuring the pressure at the focal region of the acoustic lens when driving the piezoelectric disk at 76 V and different frequencies, as shown in Fig. 4b. From the Schlieren-WFS system, the nominal resonant frequency of 2.2 MHz of the disk leads to the highest-pressure values, while the pressure progressively decreases at higher and lower frequency values. This behavior agrees with measurements using the needle hydrophone, both qualitatively and quantitatively. Again, the uncertainty of the retrieved pressure values favors the use of the Schlieren-WFS system at high pressures.

The above results highlight the excellent performance of the Schlieren-WFS system in terms of pressure sensitivity and range, comparable with that of state-of-the-art needle hydrophones. However, there is a significant difference in the way the measurements were performed for each system. In the case of the Schlieren-WFS system, an entire 3D field was captured; instead, the pressure from a single voxel was used for the hydrophone. This is due to the enormous recording speed advantage of our approach. To quantify it, we calculated the time required to take a 3D pressure measurement with the needle hydrophone and with the Schlieren-WFS system as a function of the number of pixels in the US propagation direction (z-axis). We evaluated this relation for different XY dimensions (e.g., 50 × 50, 100 × 100 and 200 × 200 pixels), as shown in Fig. 5a. Importantly, the measurement time for the Schlieren-WFS is independent of the number of pixels along z or the size of the XY slice. Note that, in all cases, we considered a tomographic reconstruction using 180 different angles, which produces an effective pixel size of 40 μm. The speed advantage of our system is mainly due to the use of a camera for pressure sensing, which provides access to millions of pixels in a single snapshot – the measurement time will remain fixed as long as the number of voxels is lower than the number of camera pixels, which is 360 × 270 in current experiments. As a simple example, let us consider the measurement time taken by the needle hydrophone system for different volumes. Considering a point-to-point dwell time of 0.2 s (5 points per second, the parameter used in our measurements), reconstructing a pressure field with 50 × 50 × 50 points would take 7 h; a 100 × 100 × 100 volume would take 56 h and a 200 × 200 × 200 measurement would last 19 days. All these times are exaggeratedly large compared to the 10 s measurement time that the Schlieren-WFS system would require in all these scenarios.

The effects of the speed advantage of the Schlieren-WFS method over a scanning hydrophone can be better illustrated in Fig. 5b. In this case, we compare the pressure maps that would be measured over a time span of 10 s using the Schlieren-WFS system as well as the needle hydrophone. The former allows a detailed reconstruction of the pressure field, with over 16 million voxels. In striking contrast, the needle hydrophone only allows retrieval of 50 voxels – again, assuming a pixel dwell time of 0.2 s. The user, though, has flexibility in selecting how to measure these 50 points. For instance, it is possible to choose the pressure points distributed across the XY plane and covering the same field of view as the Schlieren-WFS. This leads to a 7 × 7 pixel map with an extremely poor spatial resolution of 1.4 mm per pixel. The same occurs if the 7 × 7 pixel map is acquired along the XZ plane. As a result, the different pressure regions are barely distinguishable. Alternatively, it is possible to select 50 voxels spaced by 0.04 mm (along the XZ or XY plane), the same resolution as in the Schlieren-WFS system. In this case, a high-resolution pressure map can be retrieved but at the cost of covering an extremely small region of only 0.25 × 0.25 mm. Note that our needle hydrophone had a size of 0.5 mm, larger than the voxel size, and thus Fig. 5b(right) is clearly oversampled. In any case, the speed limitations of needle hydrophone measurements and its intrinsic trade-off between resolution and field-of- remain valid.

4.4. Potential limitations of the Schlieren-WFS system

The use of the Schlieren-WFS system offers promise for the quasi-real-time characterization of US fields inside water at sub-millimeter resolution. Still, several aspects need to be considered when implementing the system. As in any optical method, the non-transparency of the fluid where the US field is to be characterized can affect the measurements. Thus, the presence of scattering or absorbing particles in the fluid may produce a non-predictable effect on the light deflection and hence the wavefront detection could lead to an incorrect measurement of the phase. It is also important to note that our system performance is excellent at high pressures, but the signal-to-noise ratio worsens as the

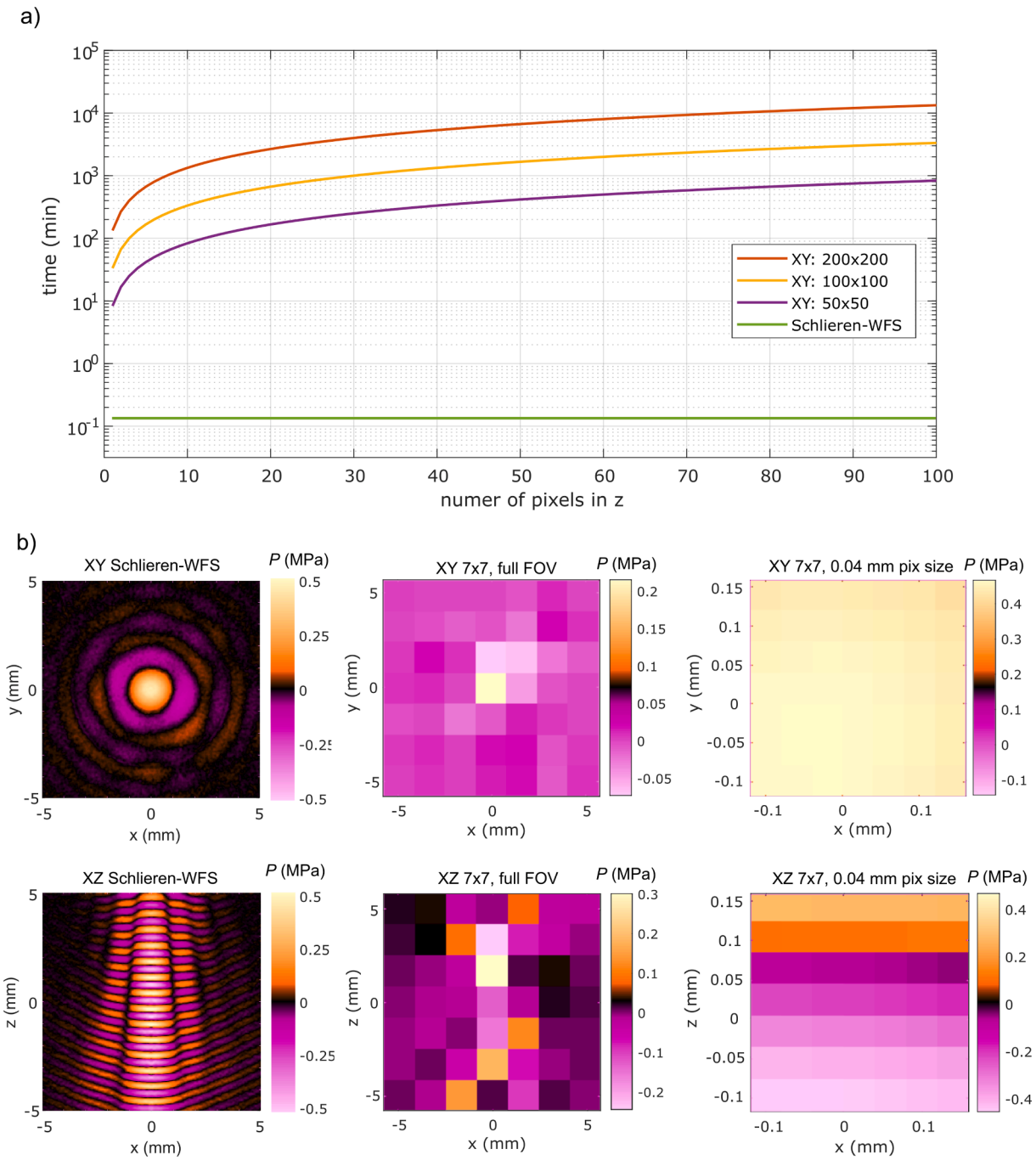


Fig. 5. Assessment of the required time for 3D pressure field measurements. a) Plot of the pressure measurement time as a function of the number of pixels considered along the *z* direction when using the needle hydrophone and different XY number of pixels, and the Schlieren-WFS system b) Experimental pressure maps obtained using an acquisition time of 10 s for: the Schlieren-WFS system with a voxel size of 40 × 40 × 40 μm (left); the needle hydrophone covering an area corresponding to the same field of view (FOV) of the Schlieren-WFS system but with a pixel size of 1.4 mm (center); the needle hydrophone with the same pixel size as in the Schlieren-WFS system but featuring a very small FOV (right).

pressure decreases. This issue can be improved by applying more binning to the Schlieren camera, at the expense of spatial resolution, or by image averaging the projections at each angle, leading to an increase in the measurement time. The current setup is also bulky, with the Schlieren arm covering a distance of about 1.5 m. Such a length improves the Schlieren sensitivity to differences in refractive index and enhances the contrast on the projections. A simple way to make the system more compact is to reduce the focal lengths of the lenses, although it comes at the cost of contrast loss. Alternatively, mirrors could be used to reduce the system length while maintaining the same optical path length. Note, though, that the Schlieren branch of the system is only used because of the small field of view and very low resolution of the WFS. With advances in microlens fabrication techniques [31] and novel cameras with larger detectors, next-generation WFS could provide the resolution and field of view to directly perform tomography with the extracted phase maps, although it may be difficult to beat the resolution of the camera used for the Schlieren setup.

5. Conclusions

The combination of Schlieren tomography with a wavefront sensor allows the calibration-free characterization of US fields at high spatial resolution. The proposed method takes advantage of the acousto-optic effect and wavefront sensing to rapidly obtain the phase projections of the US field. Through inverse reconstruction, the phase 3D pattern is recovered, and, hence, the pressure values. As our results demonstrate, this technique is suitable for quasi-real-time acquisition – more than 3 orders of magnitude faster than traditional methods based on hydrophone scanning – of US fields covering a wide range of pressures and frequencies. In contrast to other optical methods, the high detection range of the WFS allows measuring fields with pressures up to 50 MPa without the need for phase unwrapping. Furthermore, the setup obviates the need for interferometric schemes and can be implemented using standard post-processing techniques using a conventional computer. We anticipate that the Schlieren-WFS system will help to expand the portfolio of applications where ultrasound is used.

Declaration of Competing Interest

The authors declare that they have no known competing financial interests or personal relationships that could have appeared to influence the work reported in this paper.

Data availability

Data will be made available on request.

Acknowledgments

Funding: This work has been supported by the European Research Council (ERC) under the European Union's Horizon 2020 research and innovation program (grant agreement No. 101002460). M.D. is a Serra Hunter professor.

Appendix A. Supplementary data

Supplementary data to this article can be found online at https://doi.org/10.1016/j.ultras.2023.107115.

References

[1] K. Melde, A.G. Mark, T. Qiu, P. Fischer, Holograms for acoustics, Nature 537 (2016) 518–522, https://doi.org/10.1038/nature19755.
[2] J. Kim, S. Kasoji, P.G. Durham, P.A. Dayton, Acoustic holograms for directing arbitrary cavitation patterns, Appl. Phys. Lett. 118 (2021), https://doi.org/10.1063/5.0035298.
[3] X. Ren, Q. Zhou, J. Huang, Z. Xu, X. Liu, Holographic generation of arbitrary ultrasonic fields by simultaneous modulation of amplitude and phase, Ultrasonics. 134 (2023), 107074, https://doi.org/10.1016/j.ultras.2023.107074.
[4] S. Jiménez-Gambín, N. Jiménez, J.M. Benlloch, F. Camarena, Holograms to focus arbitrary ultrasonic fields through the skull, Phys. Rev. Appl. 12 (2019), 014016, https://doi.org/10.1103/PhysRevApplied.12.014016.
[5] J.E. Kennedy, High-intensity focused ultrasound in the treatment of solid tumours, Nat. Rev. Cancer. 5 (2005) 321–327, https://doi.org/10.1182/blood-2004-10-4135.
[6] Y. Hertzberg, G. Navon, Bypassing absorbing objects in focused ultrasound using computer generated holographic technique, Med. Phys. 38 (2011) 6407–6415, https://doi.org/10.1118/1.3651464.
[7] Y.H. Hsiao, S.J. Kuo, H. Der Tsai, M.C. Chou, G.P. Yeh, Clinical application of high-intensity focused ultrasound in cancer therapy, J. Cancer. 7 (2016) 225–231, https://doi.org/10.7150/jca.13906.
[8] L. Svilainis, A. Chaziachmetovas, P. Kaskonas, T.E.G. Alvarez-arenas, Ultrasonic needle hydrophone calibration in air by a parabolic off-axis mirror focused beam using three-transducer reciprocity, Ultrasonics. 133 (2023), 107025, https://doi.org/10.1016/j.ultras.2023.107025.
[9] T. Huttunen, J.P. Kaipio, A. Member, K. Hynynen, Modeling of anomalies due to hydrophones in continuous-wave ultrasound fields, 50 (2003) 1486–1500, doi:10.1109/tuffc.2003.1251132.
[10] J. Seo, N. Koizumi, K. Yoshinaka, N. Sugita, A. Nomiya, Y. Homma, Y. Matsumoto, M. Mitsuishi, Three-dimensional computer-controlled acoustic pressure scanning and quantification of focused ultrasound, IEEE Trans. Ultrason. Ferroelectr. Freq. Control. 57 (2010) 883–891, https://doi.org/10.1109/TUFFC.2010.1492.
[11] K. Melde, T. Qiu, P. Fischer, Fast spatial scanning of 3D ultrasound fields via thermography, Appl. Phys. Lett. 113 (2018), https://doi.org/10.1063/1.5046834.
[12] E. Martin, E.Z. Zhang, J.A. Guggenheim, P.C. Beard, B.E. Treeby, Rapid Spatial Mapping of Focused Ultrasound Fields Using a Planar Fabry – Pérot Sensor, IEEE Trans. Ultrason. Ferroelectr. Freq. Control. 64 (2017) 1711–1722, https://doi.org/10.1109/TUFFC.2017.2748886.
[13] D.R. Bacon, Primary calibration of ultrasonic hydrophones using optical interferometry, IEEE Trans. Ultrason. Ferroelectr. Freq. Control. 35 (1988) 152–161, https://doi.org/10.1109/58.4165.
[14] J.V. Knuuttila, P.T. Tikka, M.M. Salomaa, Scanning Michelson interferometer for imaging surface acoustic wave fields, Opt. Lett. 25 (2000) 613, https://doi.org/10.1364/ol.25.000613.
[15] A. Korpel, Acousto-optics—a review of fundamentals, Proc. IEEE. 69 (1981) 48–53, https://doi.org/10.1109/PROC.1981.11919.
[16] M. Duocastella, S. Surdo, A. Zunino, A. Diaspro, P. Saggau, Acousto-optic systems for advanced microscopy, JPhys Photonics. 3 (2021), https://doi.org/10.1088/2515-7647/abc23c.
[17] A.R. Harland, J.N. Petzing, J.R. Tyrer, Nonperturbing measurements of spatially distributed underwater acoustic fields using a scanning laser Doppler vibrometer, J. Acoust. Soc. Am. 115 (2004) 187–195, https://doi.org/10.1121/1.1635841.
[18] R. Longo, S. Vanlanduit, G. Arroud, P. Guillaume, Underwater acoustic wavefront visualization by scanning laser doppler vibrometer for the characterization of focused ultrasonic, Transducers (2015) 19925–19936, https://doi.org/10.3390/s150819925.
[19] G.S. Settles, Schlieren und shadowgraph techniques: visualizing phenomena in transparent media - Experimental Fluid Mechanics, Springer-Verlag, Berlin, 2001.
[20] D. Möller, N. Degen, J. Dual, Schlieren visualization of ultrasonic standing waves in mm-sized chambers for ultrasonic particle manipulation, J. Nanobiotechnology. 11 (2013) 1–5, https://doi.org/10.1186/1477-3155-11-21.
[21] T. Neumann, H. Ermert, Schlieren visualization of ultrasonic wave fields with high spatial resolution, Ultrasonics. 44 (2006) 1561–1566, https://doi.org/10.1016/j.ultras.2006.05.209.
[22] A.C. Kak, M. Slaney, Principles of Computerized Tomographic Imaging, IEEE, New York, 1988.
[23] X. Jiang, Q. Cheng, Z. Xu, M. Qian, Q. Han, Quantitative measurement of acoustic pressure in the focal zone of acoustic lens-line focusing using the Schlieren method, Appl. Opt. 55 (2016) 2478, https://doi.org/10.1364/ao.55.002478.
[24] G.E. Elsinga, B.W. Van Oudheusden, F. Scarano, D.W. Watt, Assessment and application of quantitative schlieren methods: calibrated color schlieren and background oriented schlieren, Exp. Fluids. 36 (2004) 309–325, https://doi.org/10.1007/s00348-003-0724-8.
[25] T. Nakamura, R. Iwasaki, S. Yoshizawa, S.I. Umemura, Quantitative measurement of ultrasonic pressure field using combination of optical phase contrast and nonlinear acoustic holography methods, Jpn. J. Appl. Phys. 57 (2018) 3–8, https://doi.org/10.7567/JJAP.57.07LB13.
[26] J. Won Cha, P.T.C. So, A shack-hartmann wavefront sensor based adaptive optics system for multiphoton microscopy, Biomed. Opt. BIOMED 2008 (15) (2008) 1–10, https://doi.org/10.1117/1.3475954.
[27] J. Liang, B. Grimm, S. Goelz, J.F. Bille, Objective measurement of wave aberrations of the human eye with the use of a Hartmann-Shack wave-front sensor, J. Opt. Soc. Am. A. 11 (1994) 1949, https://doi.org/10.1364/josaa.11.001949.
[28] W. Merzkirch, F. Visualization, A. Press, New York (1974), https://doi.org/10.1016/B978-0-08-102437-9.00016-4.
[29] J.N. Caron, G.P. DiComo, Frequency response of optical beam deflection by ultrasound in water, Appl. Opt. 53 (2014) 7677, https://doi.org/10.1364/ao.53.007677.
[30] B.E. Treeby, J. Budisky, E.S. Wise, J. Jaros, B.T. Cox, Rapid calculation of acoustic fields from arbitrary continuous-wave sources, J. Acoust. Soc. Am. 143 (2018) 529–537, https://doi.org/10.1121/1.5021245.
[31] S. Surdo, R. Carzino, A. Diaspro, M. Duocastella, Single-shot laser additive manufacturing of high fill-factor microlens arrays, Adv. Opt. Mater. 6 (2018) 1–9, https://doi.org/10.1002/adom.201701190.